Ab initio ground potential energy surface and quasiclassical trajectory study of the $O(^1D)+CH_4(X\,^1A_1)\rightarrow OH(X\,^2\Pi)+CH_3(X\,^2A_2'')$ reaction dynamics

Miguel González[a] and Jordi Hernando
Departament de Química Física i Centre de Recerca en Química Teòrica, Universitat de Barcelona. C/Martí i Franquès, 1. 08028 Barcelona, Spain

Irene Baños
Departamento de Química, Universidad de La Rioja. C/Obispo Bustamante, 3. 26004 Logroño, Spain

R. Sayós[b]
Departament de Química Física i Centre de Recerca en Química Teòrica, Universitat de Barcelona. C/Martí i Franquès, 1. 08028 Barcelona, Spain

(Received 1 February 1999; accepted 18 August 1999)

An *ab initio* study of the ground potential energy surface (PES) of the $O(^1D)+CH_4\rightarrow OH+CH_3$ reaction has been performed using the second and fourth order Møller–Plesset methods with a large basis set. From the *ab initio* data a triatomic analytical ground PES with the methyl group treated as an atom of 15.0 amu has been derived. This PES has been employed to study the dynamics of the reaction by means of the quasiclassical trajectory (QCT) method. A good agreement between the experimental and QCT OH rovibrational distributions at a collision energy of 0.212 eV with the methane molecule at 298 K has been obtained. The analysis of the microscopic reaction mechanism shows that the reaction takes place almost exclusively through the insertion of the $O(^1D)$ atom into a C–H bond, due to the presence of the deep $(CH_3)OH$ minimum, and the resulting trajectories may be direct or nondirect (short-lived collision complexes mainly) with about the same probability. The OH vibrational distribution arising from the direct mechanism is inverted, while the nondirect mechanism leads to a noninverted one. There is some tendency to give broader OH rotational distributions peaking at higher N' values, particularly for the vibrational levels $v'=0-1$, in the case of the nondirect trajectories. The PES derived here may be used in dynamics studies under conditions where the methyl group motions are not strongly coupled to the motions leading to reaction. © *1999 American Institute of Physics.* [S0021-9606(99)30442-6]

I. INTRODUCTION

The reactions of the oxygen atom in the first excited electronic state $(O(^1D))$ with alkanes, and specially with CH_4, are relevant in stratospheric chemistry in the context of ozone degradation through the OH/HO_2 catalytic cycle.[1–3] Furthermore, its highly different reactive behavior with respect to the ground state oxygen atom $(O(^3P))$ makes the study of this kind of systems particularly interesting. Thus, for instance, $O(^1D)$ is claimed to react very efficiently with compounds containing X–H bonds (such as H–H, C–H, N–H, and O–H), by both abstraction and, mainly, insertion mechanisms, in contrast to what happens to $O(^3P)$.

The aim of this work is to study theoretically the ground potential energy surface (PES) and dynamics of the gas phase reaction of $O(^1D)$ with CH_4,

$$O(^1D)+CH_4(X\,^1A_1)\rightarrow OH(X\,^2\Pi)+CH_3(X\,^2A_2'') \qquad (1)$$

$$\Delta H^0_{298\ K}=-43.1\ \text{kcal mol}^{-1}\ \text{(Ref. 4)}.$$

This reaction has been extensively studied using different experimental techniques. The global (including all possible reaction channels) thermal rate constant for $O(^1D)+CH_4$ is very large, approaching the gas kinetic value. The recommended global rate constant (k) value is $1.5\times10^{-10}\,\text{cm}^3\,\text{molecule}^{-1}\,\text{s}^{-1}$ over the temperature range 200–300 K.[5] This suggests that the reaction does not have activation energy, in contrast to what happens for the analogous reaction with $O(^3P)$, which exhibits a high activation energy (see, e.g., Ref. 6). At room temperature, the following product branching ratios were measured:[7] $\Phi(OH(X\,^2\Pi)+CH_3(X\,^2A_2''))=0.9$ $(+0.1,-0.2)$, $\Phi(CH_2O(X\,^1A_1)+H_2(X\,^1\Sigma_g^+)$ and $\Phi(CH_2O(X\,^1A_1)+H(^2S)+H(^2S))=0.06\pm0.01$, $\Phi(CH_2(a\,^1A_1)+H_2O(X\,^1A_1))=0.02\pm0.01$, and $\Phi(O(^3P)+CH_4(X\,^1A_1))=0.02\pm0.01$. The H-atom product yield has been reported,[8–10] and in a crossed molecular beams experiment the H atom and H_2 molecule channels have been investigated.[11]

The measurement of the $OH(X\,^2\Pi)$ vibrational[12–18] and rotational[12,15–19] distributions arising from reaction (1) has been carried out using mainly laser induced fluorescence (LIF) to probe this molecule. The $O(^1D)$ atom was generated by photodissociation of either N_2O (193 nm) or O_3 (248 nm or 266 nm), allowing in some cases for $O(^1D)$ thermalization. Therefore, nascent $OH(X\,^2\Pi)$ rovibrational populations

[a]Author to whom correspondence should be addressed. Electronic mail: miguel@qf.ub.es
[b]Author to whom correspondence should be addressed. Electronic mail: r.sayos@qf.ub.es

considering different $O(^1D)+CH_4$ collision energy distributions have been determined. However, the change of relative translational energies did not modify in an important extent the OH energy distributions obtained for this radical. This is probably due to the large reaction exothermicity, which attenuates the influence of the initial conditions on the available energy in products. Thus, e.g., for the $O(^1D)+CH_4$ reaction photoinitiated by photolysis of N_2O (193 nm) and O_3 (248 nm), the average collision energies are, respectively, 0.403 and 0.212 eV, while the corresponding available energies in products are 2.30 and 2.11 eV. Vibrational populated levels up to $v'=4$ with a relatively flat vibrational distribution for $v'=0$, 1, 2, and 3 have been determined using the O_3 photodissociation at 248 nm (Refs. 13,15) and 266 nm.[14] A bimodal rotational distribution has been observed essentially for $v'=0$, which was thought to be due to the coexistence of two different microscopic reaction mechanisms.[12,15–18] The $OH(X\,^2\Pi_{3/2})/OH(X\,^2\Pi_{1/2})$ spin–orbit population ratio is statistical,[12,15–18] and the $\Pi(A')/\Pi(A'')$ lambda doublet population ratio is larger than one,[12,15,16,18] both in contrast to what happens for the analogous reaction with $O(^3P)$. The stereodynamics of reaction (1) has also been examined[19–23] using polarized Doppler-resolved LIF spectroscopy. The differential cross section (DCS) have been determined for two rovibrationals levels of $OH(X\,^2\Pi)$, $(v'=0, N'=5)$ and $(v'=4, N'=8)$. The asymmetric and mainly backward peaked DCS obtained for the scattering of $OH(v'=0, N'=5)$ contrasts to the near symmetric DCS of $OH(v'=4, N'=8)$.

The vibrational[24,25] and rotational[25] distributions of the CH_3 molecules produced in reaction (1) have also been measured. The vibrational distributions in the ν_1 (symmetric stretch) and ν_2 (''umbrella'' mode) modes are noninverted, with the ν_2 mode much less excited than statistically expected. The rotational distribution is much hotter than the corresponding at room temperature. The lifetime (τ approximately 3 ps) of the CH_3OH intermediate produced after the 267 nm photolysis of the $CH_4\cdot O_3$ van der Waals cluster[26] and the reaction of $O(^1D)$ with CH_4 clusters[16] have also been studied. Experimental information is also available for the reactions of $O(^1D)$ with larger alkanes such as, e.g., C_2H_6 and C_3H_8.[9,12,15–18,25] It is worthwhile to point out that the yield of the reaction channel leading to $OH(X\,^2\Pi)+$alkyl radical is very much lower for these reactions than for the reaction with CH_4.[15] This is due to the important role that the cleavage of the weaker C–C bonds plays in the reactivity of these systems.

Despite of the abundant experimental information available on the $O(^1D)+CH_4$ reaction, theoretical studies are very scarce. There is an *ab initio* study at the CCI//CASSCF level on the CH_2+H_2O, $HCOH+H_2$, and CH_2O+H_2 reaction channels,[27] which may be possible through the methanol fragmentation. Another *ab initio* study at the MRCI//CASSCF level focused on the description of the $OH+CH_3$ and CH_3O+H products that also correlate with CH_3OH.[28] In this context, an *ab initio* characterization of the ground PES of the $O(^1D)+CH_4\rightarrow OH+CH_3$ reaction has been performed in this work. As a first approximation, a triatomic analytical representation of this PES has been derived and a quasiclassical trajectory (QCT) dynamics study of the reaction has been performed. To the best of our knowledge this represents the first theoretical study carried out on the dynamics of this reaction.

This work is organized as follows. Section II deals with the *ab initio* calculations and fitting of the ground PES, and Sec. III shows the QCT OH rovibrational distributions and the influence of the microscopic reaction mechanism on them. In Sec. IV the concluding remarks are given.

II. POTENTIAL ENERGY SURFACE

A. *Ab initio* calculations

For C_1, C_s, and C_{3v} symmetries, the following PES correlate with the asymptotic regions of reaction (1): (a) reactants: (5) ^1A (C_1), (3) $^1A'+(2)$ $^1A''$ (C_s) and (2) $^1E+{}^1A_1$ (C_{3v}); (b) products: (2) $^1A+(2)$ ^3A (C_1), $^1A'+{}^1A''+{}^3A'+{}^3A''$ (C_s) and $^1E+{}^3E$ (C_{3v}). Hence, both asymptotes may correlate adiabatically through the following PES: (2) ^1A (C_1), $^1A'+{}^1A''$ (C_s) and ^1E (C_{3v}). Although the C_1 symmetry is the most important one for theoretical studies on the dynamics of reactions that involve four or more atoms, we have also taken into account higher symmetries since, as it will be shown below, the $O\cdots H\cdots CH_3$ saddle point and the CH_3OH alcohol minimum of reaction (1), obtained by insertion of the $O(^1D)$ atom into a C–H bond, have C_s geometries.

The *ab initio* study has been focused on the ground PES ($1\,^1A'$ in C_s) of reaction (1), and the GAUSSIAN 94 package of programs[29] has been used. Since in most regions of the PES the system behaves as an open-shell singlet (only around the closed-shell CH_3OH alcohol minimum the wave function is single-determinantal), the most suitable *ab initio* methods to deal with this system are those that include more than one reference determinant to describe the wave function, e.g., the CASSCF and MRCI methods. However, although these methods are nowadays accessible for the characterization of stationary points, benchmark calculations with molecular correlated wave functions on simple triatomic reactions, such as $O+H_2$,[30] $F+H_2$,[30,31] and $H+HCl$,[30] have shown that only using very large wave functions and basis sets it is possible to achieve energy values close to the experimental data. Also, in a MRCI//CASSCF calculation on the $O(^1D)+CH_4$ system using a split-valence plus polarization functions basis set (50 basis functions),[28] the relative energies of the CH_3OH minimum, CH_3O+H and CH_2OH+H from reactants present important differences with the experimental values. This type of highly accurate calculations are computationally very expensive, specially when the characterization of a reaction with a large number of atoms and electrons is intended. However, it has been shown that, under certain conditions, single-determinantal *ab initio* methods, such as the Møller–Plesset perturbational and DFT methods, can reproduce quite satisfactorily the energetics of this type of systems when the ''broken symmetry'' approach is considered.[32,33] The use of this approach leads to energy values lying between the triplet and open-shell singlet ones, due to the existence of a large spin contamination. The elimination of the spin contamination of the wave function

TABLE I. Energetics of the system using different methods and basis sets.

Method	E+ZPE/kcal mol^{-1} [a,b]		
	CH_3OH minimum	CH_3+OH	CH_3O+H
PUMP2//UMP2/6-311G($2df$,$2pd$)	−128.0(−132.2)	−45.6(−40.6)	−28.9(−24.0)
PUMP4//UMP2/6-311G($2df$,$2pd$)	−129.2(−133.5)	−42.6(−38.6)	−28.0(−23.1)
PUMP2//UMP2/6-311G($3d2f$,$3p2d$)	−131.9(−136.1)	−47.1(−43.1)	−31.0(−26.1)
PUMP4//UMP2/6-311G($3d2f$,$3p2d$)	−133.4(−137.6)	−45.2(−41.2)	−30.3(−25.4)
Experimental data	−133.9[c]	−43.5[c]	−31.1[d]

[a]Energy referred to reactants. The values in parentheses correspond to the energies without including the UMP2 ZPE.

[b]Absolute values of energy (hartrees) for $O(^1D)+CH_4$ are −115.360 577 (UMP2/6-311G($2df$,$2pd$)), −115.340 479 (PUMP2//UMP2/6-311G($2df$,$2pd$)), −115.374 221 (PUMP4//UMP2/6-311G($2df$,$2pd$)), −115.372 652 (UMP2/6-311G($3d2f$,$3p2d$)), −115.353 367 (PUMP2//UMP2/6-311G($3d2f$,$3p2d$)), and −115.386 403 (PUMP4//UMP2/6-311G($3d2f$,$3p2d$)).

[c]$\Delta H^0_{0\,K}$ (Ref. 4).

[d]$\Delta H^0_{0\,K}$ (Refs. 4 and 28).

becomes a critical aspect. Fortunately, an efficient projection algorithm[32] to remove the spin contamination when Møller–Plesset perturbational methods are used is included in the GAUSSIAN 94 package.[29]

We have selected as a suitable method of calculation the unrestricted second-order Møller–Plesset perturbation theory (UMP2) method using the 6-311G($2df$,$2pd$) basis set (116 basis functions), UMP2/6-311G($2df$,$2pd$) *ab initio* level hereafter, to locate the stationary points and connections between them. The geometry optimizations and frequency calculations have been performed at this level, although to determine the saddle point geometry also a more sophisticated treatment have been used. The energies of the set of *ab initio* points of the PES required to obtain, as a first approximation, a triatomic analytical representation have been calculated at the spin projected unrestricted fourth-order Møller–Plesset perturbation theory (PUMP4) method using the same basis set, PUMP4/6-311G($2df$,$2pd$) *ab initio* level hereafter. The spin projected method has been employed to eliminate the spin contamination of the PES ($0.00<\langle S^2\rangle/\hbar^2<1.10$). The strategy used to characterize the PES has been the following: first, the stationary points of the PES (reactants, products, saddle point, and minimum) have been optimized at the UMP2/6-311G($2df$,$2pd$) level; after this, the connections between these stationary points and some additional points (specially, $O–H–CH_3$ saddle point and $H–O–CH_3$ minimum bending curves) have been calculated at the UMP2/6-311G($2df$,$2pd$) level, optimizing the geometry of the methyl group; finally, the energy of each point previously calculated at the UMP2/6-311G($2df$,$2pd$) level has been computed using the PUMP4/6-311G($2df$,$2pd$) method. Each optimization (UMP2) plus single point energy calculation (PUMP4) takes typically about 2.5 h of CPU time on a single processor of a Silicon Graphics O2000 workstation with 512 Mbyte of RAM. In the next paragraphs the present *ab initio* results will be compared with experimental data and previous *ab initio* calculations.

The energetics of the system using different methods and basis sets is shown in Table I, considering the CH_3OH alcohol minimum and those asymptotes relevant to the triatomic model of reaction (1). No significant differences appear when the 6-311G($2df$,$2pd$) basis set is used instead of the larger 6-311G($3d2f$,$3p2d$) one. In fact, the methods selected here, the UMP2/6-311G($2df$,$2pd$) and PUMP4//UMP2/6-311G($2df$,$2pd$) methods for, respectively, geometries and frequencies, and energies (including the UMP2 zero point energy (ZPE) when necessary), are the ones which best reproduce the exothermicity of reaction (1), and predict the exothermicity of the minor channel CH_3O+H and depth of the CH_3OH alcohol minimum with deviations of, respectively, 10% and 3.5% with respect to experimental data. The results obtained for the geometries and frequencies of the CH_4, CH_3, OH, and CH_3O molecules also show a good agreement with experiments, although instead of a C_{3v} structure a C_s geometry is predicted for CH_3O (Table II).

The structures of the two stationary points located between reactants and products on the ground $^1A'$ PES ($O\cdots H\cdots CH_3$ saddle point and CH_3OH alcohol minimum) are plotted in Fig. 1. Their properties are indicated in Tables III (geometry and energy) and IV (frequencies). The UMP2/6-311G($2df$,$2pd$) optimization and the PUMP4//UMP2/6-311G($2df$,$2pd$) energy calculation of the CH_3OH minimum have provided quite satisfactory results when they are compared with experimental data. Thus, the *ab initio* structure and frequencies are in good agreement with experiments (see, respectively, Refs. 34 and 39) and, as it was mentioned above, only a 3.5% of deviation exists between the *ab initio* and experimental[4] depth of the minimum with respect to reactants (including ZPE).

Some more efforts have been devoted to the $O\cdots H\cdots CH_3$ saddle point characterization. This stationary point was previously computed using the CASSCF (geometry) and MRCI (energy) methods.[28] In the UMP2/6-311G($2df$,$2pd$) and CASSCF calculations an early saddle point with an almost unaltered structure of the CH_4 molecule and the $O(^1D)$ atom approaching collinearly to a C–H bond is found. However, the UMP2/6-311G($2df$,$2pd$) optimization yields a much shorter $O\cdots H$ distance and a longer $H\cdots CH_3$ distance, with an energy barrier nearly five times higher without considering ZPE. When the projected PUMP2/6-311G($2df$,$2pd$) method is used, the energy of the

TABLE II. Geometry and harmonic frequencies of the reactants and products molecules.[a]

CH_4 $X\,^1A_1$ (T_d)						
R_{CH}/Å	this work	1.084				
	experiment[c]	1.0870_7				
ν/cm^{-1}	this work	1350.3 (T_2)	1590.6 (E)	3085.7 (A_1)	3222.8 (T_2)	
	experiment[d]	1306.0	1534.0	2916.5	3018.7	
CH_3 $X\,^2A_2''$ (D_{3h})						
R_{CH}/Å	this work	1.073				
	experiment[c]	1.0767				
ν/cm^{-1}	this work	474.2 (A_2'')	1446.1 (E')	3189.8 (A_1')	3381.5 (E')	
	experiment[d]	580	1383	3002	3184	
OH $X\,^2\Pi$ $(C_{\infty v})$						
R_{OH}/Å	this work	0.963				
	experiment[e]	0.96966				
ν/cm^{-1}	this work	3870.3 (Σ^+)				
	experiment[e]	3737.76_1				
CH_3O $X\,^2A'$ (C_s)[b]						
R_{CO}, $R_{CH'}$, $R_{CH''}$/Å	this work	1.368	1.097	1.091		
	experiment[f]	1.3637	1.0958	1.0958		
$\angle$H′CO, $\angle$H″CO/°	this work	105.2	113.1			
	experiment[f]	111.27	111.27			
ν/cm^{-1}	this work	806.3 (A'')	975.0 (A')	1146.5 (A')	1412.6 (A')	1430.0 (A'')
		1542.7 (A')	3018.1 (A')	3097.2 (A')	3137.1 (A'')	

[a]See Fig. 1 for the internal coordinates definition. The *ab initio* geometries and harmonic frequencies have been determined at the UMP2/6-311G($2df$,$2pd$) level.
[b]Experimental distances and angles between effective nuclear positions derived from isotopic differences in rotational constants (Ref. 37). The reported experimental geometry is C_{3v} ($X\,^2E$), although the Jahn–Teller effect should lead to a C_s structure probably not far from C_{3v}. However, the *ab initio* calculations lead to a C_s structure (see text and, e.g., Ref. 38). This result comes out without including the Jahn–Teller vibronic coupling in the calculation.
[c]Reference 34.
[d]Reference 35.
[e]Reference 36.
[f]Reference 37.

UMP2/6-311G($2df$,$2pd$) saddle point falls below the reactants asymptote and, therefore, the barrier above reactants disappears. Nevertheless, a barrier is observed when additional points are calculated at the projected level along the $O\cdots H\cdots CH_3$ reaction coordinate, with the same O–H–C angle as the one found for the UMP2/6-311G($2df$,$2pd$) saddle point. Thus, at the projected level the existence of a barrier is observed. This means that the projected saddle point is shifted with respect to the unprojected one due to the spin contamination ($\langle S^2\rangle/\hbar^2$ equals 1.0 for these points) which affects, as indicated before, the ''broken symmetry'' unrestricted solution.

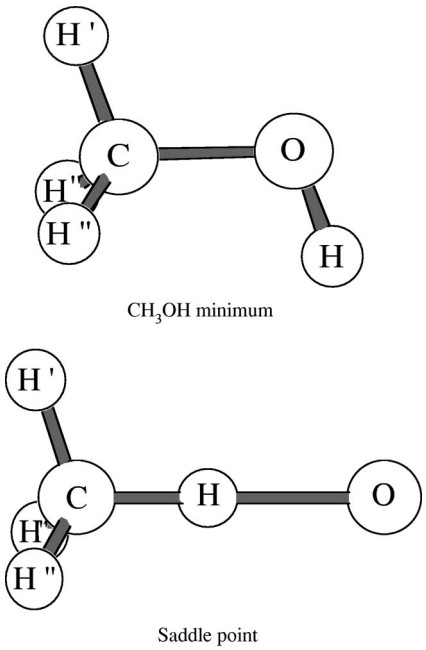

FIG. 1. $O\cdots H\cdots(CH_3)$ saddle point and CH_3OH minimum structures.

Since in the GAUSSIAN 94 package[29] there are no available neither analytical nor numerical algorithms to optimize stationary points at any projected level, the strategy employed to determine the PUMP4/6-311G($2df$,$2pd$) saddle point was the following: first, a set of 32 points along the reaction coordinate $O\cdots H\cdots CH_3$, fixing the O–H–C angle to that of the UMP2/6-311G($2df$,$2pd$) saddle point, were calculated by optimizing the structure of the methyl group at the UMP2/6-311G($2df$,$2pd$) level and computing, after this, the PUMP4/6-311G($2df$,$2pd$) energy; second, these points were fitted using bicubic splines in terms of the R_{O-H} and R_{H-C} distances and the resulting values of these two distances for the projected saddle point were derived; finally, the structure of the methyl group was optimized using the UMP2/6-311G($2df$,$2pd$) method, keeping fixed R_{O-H}, R_{H-C}, and the O–H–C angle. The energy of the final structure was computed at the PUMP4/6-311G($2df$,$2pd$) level. The geometry and energy of the PUMP4/6-311G($2df$,$2pd$) saddle point calculated in this way show a quite good agree-

TABLE III. Geometry and energy of the $O\cdots H\cdots CH_3$ saddle point and CH_3OH minimum.[a]

Stationary point	R_{OH}/Å	R_{HC}/Å	$R_{H'C}$/Å	$R_{H''C}$/Å	∠CHO/°	∠H′CH/°	∠H″CH/°	∠H′CHO/°	E+ZPE/kcal mol^{-1}
Saddle point									
This work[b] $^1A'$									
UMP2	1.329	1.182	1.082	1.082	179.9	105.9	106.2	0.0	6.3 (10.0)
PUMP2//UMP2									−8.0 (−4.3)
PUMP4[c]	1.513	1.140	1.083	1.083	179.9	108.2	108.4	0.0	−0.1 (3.6)
Ref. 28[d] ^1E	1.66	1.10	1.08	1.08	180.0	108.7	108.7		(2.1)
Experiment[e]									≈0
Minimum									
This work[b] $^1A'$									
PUMP4//UMP2	0.956	1.928	1.085	1.091	44.3	135.2	97.6	0.0	−129.2 (−133.5)
Ref. 28[d] $^1A'$									−122.2 (−125.8)
Experiment[f]	0.9630	1.9481	1.0937	1.0937	43.9	140.0	96.4	0.0	−133.9

[a]See Fig. 1 for the internal coordinates definition. Energy referred to reactants and the values in parentheses correspond to the energies without including ZPE.
[b]The *ab initio* calculations have been done using the 6-311G/(2*df*,2*pd*) basis set, and the ZPE have been computed at the UMP2 level.
[c]The PUMP4 geometry and energy of the saddle point were obtained using bicubic splines (see text).
[d]Geometries and energies calculated, respectively, by the *ab initio* CASSCF and MRCI//CASSCF methods using a split-valence (9*s*5*p*)/[3*s*2*p*] basis set of Huzinaga–Dunning–Raffenetti plus *d* polarization functions for C and O atoms and *p* polarization functions for H atoms. ZPE for CH_3OH computed from experimental frequencies.
[e]Experimental activation energy (*T*: 200–300 K) (Ref. 5).
[f]Geometry from Ref. 34 and the energy corresponds to $\Delta H^0_{0\,K}$ (Ref. 4).

ment with the MRCI//CASSCF *ab initio* data[28] (Table III). At the projected level, an earlier saddle point structure and a much lower barrier are found than when the unprojected method is used. On the other hand, if the ZPE is included at the UMP2/6-311G(2*df*,2*pd*) level as a reasonable approximation, the PUMP4/6-311G barrier over reactants disappears. This likely would also happen in the saddle point of Ref. 28 if the ZPE was computed, and is consistent with the experimental evidence that the rate constant is independent of the temperature over the 200–300 K temperature range,[5] which suggests that there is no activation energy for reaction (1). The O–H–C angle found for the UMP2/6-311G(2*df*,2*pd*) saddle point is not exactly 180°, differing from Ref. 28. Nevertheless, although we have obtained a slightly distorted C_{3v} structure, just as it happens in the related $O(^3P)+CH_4$ system (see, e.g., Ref. 6), it should be emphasized that this result comes out from a purely electronic calculation, i.e., without including the Jahn–Teller vibronic coupling.

Once the saddle point and minimum were optimized, the connections between them and the reactants ($O(^1D)+CH_4$) and two possible reaction channels ($OH+CH_3$ and $H+CH_3O$) of the triatomic model were studied. The PUMP4//UMP2/6-311G(2*df*,2*pd*) minimum energy path (MEP) calculated for reaction (1) follows a collinear approach of the $O(^1D)$ atom to a $H–CH_3$ bond until reaching the saddle point structure. The MEP after the saddle point structure leads directly to the formation of the $OH+CH_3$ products (abstraction mechanism). However, the insertion of the $O(^1D)$ atom into a C–H bond to yield the CH_3OH minimum is also possible thanks to the $O–H–CH_3$ bending motion around the saddle point structure, the evolution of the reaction through the CH_3OH minimum being easily accessible. Once this minimum is formed, it can lead to $OH+CH_3$ or $H+CH_3O$ without any barrier over products. These results agree with those reported in Ref. 28. The competition between the two clearly different microscopic reaction mechanisms (abstraction vs insertion) will be discussed in Sec. III (QCT dynamics study).

TABLE IV. Harmonic normal mode vibrational frequencies (in cm^{-1}) for the $O\cdots H\cdots CH_3$ saddle point and CH_3OH minimum.

	Saddle point	Minimum	
Mode	*ab initio*[a]	*ab initio*[a]	Experiment[b]
ν_1	3262.1 (A')	3932.4 (A')	3681 (A')
ν_2	3251.9 (A'')	3188.6 (A')	3000 (A')
ν_3	3125.6 (A')	3125.3 (A'')	2960 (A'')
ν_4	1483.6 (A')	3059.9 (A')	2844 (A')
ν_5	1407.6 (A'')	1539.0 (A')	1477 (A')
ν_6	1293.6 (A')	1521.9 (A'')	1477 (A'')
ν_7	1211.1 (A')	1499.9 (A')	1455 (A')
ν_8	1151.7 (A'')	1395.3 (A')	1345 (A')
ν_9	778.3 (A')	1190.9 (A'')	1165 (A'')
ν_{10}	298.6 (A')	1116.4 (A')	1060 (A')
ν_{11}	143.0 (A'')	1076.1 (A')	1033 (A')
ν_{12}	1860.3*i* (A')	312.7 (A'')	200–295 (A'')

[a]UMP2/6-311G(2*df*,2*pd*) level.
[b]Reference 39. ν_{12} (torsion) is experimentally undefined because of the large coupling between internal and overall rotations.

B. Analytical potential energy surface

To describe the ground PES ($1\,^1A'$ under C_s symmetry) of reaction (1), a triatomic model where the CH_3 radical is treated as a single atom ((CH_3)) of 15 amu placed in the center of mass has been considered. This model has been used previously with quite good results, e.g., in our recent study on the $O(^3P)+CH_4$ related system.[6] The same type of analytical expression (many-body expansion[40]) and programs[41,42] used by us in Ref. 6 and in other works [e.g., $N(^4S)+NO$,[43] $O(^3P)+CS$,[44] $H(^2S)+Cl_2$ and $Cl(^2P)$

+HCl (Ref. 45) and $N(^4S)+O_2$ (Ref. 46) reactions] have also been employed here. The analytical triatomic PES model has been represented as

$$V(R_1,R_2,R_3)=V^{(2)}_{OH}(R_1)+V^{(2)}_{H(CH_3)}(R_2)+V^{(2)}_{O(CH_3)}(R_3)+V^{(3)}_{OH(CH_3)}(R_1,R_2,R_3), \quad (2)$$

where $V^{(2)}$ and $V^{(3)}$ are the two-body and three-body terms, respectively, and R_1, R_2, R_3 are the O–H, H–(CH_3), and O–(CH_3) distances.

The three asymptotic channels of the $^1A'$ PES do not correlate with the same electronic state of the O atom. The first excited state of the oxygen atom, $O(^1D)$, correlates with reactants, while the ground state, $O(^3P)$, correlates with OH and $O(CH_3)$. Due to this, a modified form of the usual many-body Eq. (2), including monoatomic terms $V^{(1)}$ and a switching term in the three-body part of the expression, should be used.[40] Nevertheless, this can be avoided if in the fitting of the two-body terms (diatomic potential energy curves) the dissociation limits of those molecules that correlate with $O(^3P)$ are altered so as to reproduce ''artificial'' dissociation limits leading to $O(^1D)$. This approximation only changes the high energy part of the diatomic curves, and the low and intermediate energy regions explored in the most usual dynamics calculations remain almost unaltered. Hence, we have used here modified dissociation energies (D_e) for the OH and $O(CH_3)$ molecules by summing up the $O(^1D)-O(^3P)$ energy difference to the corresponding D_e values describing the dissociation up to $O(^3P)$.

The diatomic potential energy curves have been fitted using an extended-Rydberg potential up to third order,

$$V^{(2)}(\rho)=-D_e(1+a_1\rho+a_2\rho^2+a_3\rho^3)e^{-a_1\rho}, \quad (3)$$

where D_e and R_e are, respectively, the dissociation energy [altered for OH and $O(CH_3)$ as indicated above] and equilibrium bond length of the corresponding diatomic or pseudodiatomic molecule, and ρ is defined as being equal to $R-R_e$. The optimal a_i diatomic parameters have been obtained for each molecule using a nonlinear least-squares procedure[41] by fitting a set of nine diatomic (PUMP4) or pseudodiatomic (PUMP4//UMP2) *ab initio* points calculated around the equilibrium distance. For the X–(CH_3) species (X=H,O) the CH_3 *ab initio* geometry was optimized in all points of the X–(CH_3) pseudodiatomic curve. The extended-Rydberg function provides a very good fitting in all cases. The optimal diatomic parameters are shown in Table V, and the spectroscopic constants derived from them for the OH, $H(CH_3)$, and $O(CH_3)$ molecules are given in Table VI.

The three-body term consists of a third-order polynomial ($P(\rho_1,\rho_2,\rho_3)$) and a range function ($T(\rho_1,\rho_2,\rho_3)$). The polynomial is expressed in terms of three internal coordinates (ρ_1,ρ_2,ρ_3), defined as $\rho_i=R_i-R_i^0$, where the selected reference structure (R_1^0,R_2^0,R_3^0) corresponds to the average between the saddle point and minimum geometries. The range function cancels the three-body term as one of the three atoms is separated from the other two. Thus, we have

$$V^{(3)}_{OH(CH_3)}(\rho_1,\rho_2,\rho_3)=P(\rho_1,\rho_2,\rho_3)T(\rho_1,\rho_2,\rho_3), \quad (4)$$

TABLE V. Optimal parameters for the analytical triatomic PES.

Two-body terms[a]	a_1/Å^{-1}		a_2/Å^{-2}		a_3/Å^{-3}
O–H	3.8782		3.6827		5.2431
H–(CH_3)	4.1842		5.2347		4.7665
O–(CH_3)	4.4502		7.0280		9.8229
Three-body term[b]					
c_{000}	5.1533	c_{300}	1.7585	γ_1	1.4159
c_{100}	4.0524	c_{210}	0.76056		
c_{010}	−2.9651	c_{201}	−2.6905	γ_2	1.6055
c_{001}	3.1605	c_{120}	8.0029		
c_{200}	1.1110	c_{111}	4.9650	γ_3	1.9616
c_{110}	5.8902	c_{102}	−2.6699	R^0_{OH}	1.2345
c_{101}	−0.19243	c_{030}	2.2627		
c_{020}	0.84014	c_{021}	−4.9220	$R^0_{H-(CH_3)}$	1.6037
c_{011}	0.35484	c_{012}	−4.5387		
c_{002}	4.3136	c_{003}	2.0029	$R^0_{O-(CH_3)}$	2.1053

[a]The dissociation energies and equilibrium distances used in the fitting are given in Table VI.
[b]Units are c_{ijk}/eV Å$^{-(i+j+k)}$, γ_i/Å^{-1}, R_i/Å.

where

$$P(\rho_1,\rho_2,\rho_3)=\sum_{i,j,k=0}^{0\leq i+j+k\leq 3} c_{ijk}\rho_1^i\rho_2^j\rho_3^k \quad (5)$$

with i, j, and k positive integer numbers, and

$$T(\rho_1,\rho_2,\rho_3)=\prod_{i=1}^{3}\left[1-\tanh\left(\frac{\gamma_i\rho_i}{2}\right)\right]. \quad (6)$$

The 20 linear parameters $\{c_{ijk}\}$ and three nonlinear ones $\{\gamma_i\}$ of the three-body term have been determined by a weighted nonlinear least-squares procedure,[42] using the $O\cdots H\cdots(CH_3)$ saddle point, $(CH_3)OH$ minimum and 124 additional *ab initio* points of different regions of the $^1A'$ PES: MEP from $O(^1D)+H-(CH_3)$ to $OH+(CH_3)$ (30 points), which is essentially collinear (179°–180°), connections of the (CH_3)–O–H minimum with $O(^1D)+H-(CH_3)$ (22 points), O–H+(CH_3) (22 points) and (CH_3)–O+H (25 points), as well as some additional grids of points in other regions of interest of the PES (16 points describing the bending curves around the saddle point and minimum). In the fitting, a weight of 1.0 was used for each one of these points and for the first-partial derivatives of the energy (equal to zero) with respect to, respectively, R_{OH}, $R_{H(CH_3)}$, and the O–H–(CH_3) angle at the saddle point and minimum geometries. Moreover, nine points corresponding to the $O(^1D)$ approach on the (CH_3) side were also considered (weight =1.0). As previously indicated (cf. Sec. II A), the methyl group structure of each one of these points were optimized at the UMP2/6-311G($2df$,$2pd$) level. The saddle point and minimum structures were determined using the PUMP4/6-311G($2df$,$2pd$) and UMP2/6-311G($2df$,$2pd$) methods, respectively. In all cases the energy was computed at the PUMP4/6-311G($2df$,$2pd$) level. The optimal three-body parameters and the properties of the $O\cdots H\cdots(CH_3)$ saddle point and $(CH_3)OH$ minimum of the analytical PES are given, respectively, in Tables V and VII. Furthermore, $^1A'$ equipotential contour curves for three different O–H–(CH_3) approach angles and the connection of the

TABLE VI. Properties of the diatomic and pseudodiatomic molecules.

Species	D_e/eV[a]	R_e/Å[b]	ν_e /cm^{-1}	$\nu_e x_e$ /cm^{-1}	B_e /cm^{-1}	α_e /cm^{-1}
O–H						
Analytical fit	6.4659 (4.5459+1.9200)	0.9634	3772.8	99.69	19.16	0.9408
Experiment[c]	6.587 (4.621+1.966)	0.96966	3737.76_1	84.881_3	18.910_8	0.7242
H–(CH_3)						
Analytical fit	4.7922	1.1566	3116.1	48.69	13.34	0.4776
Experiment	4.820[d]	1.1562[e]				
O–(CH_3)						
Analytical fit	5.7931 (3.8731+1.9200)	1.4444	1080.8	4.726	1.042	0.1799×10^{-1}
Experiment	6.03[f] (4.06+1.966)	1.4407[g]				

[a]*Ab initio* D_e for O–H and O–(CH_3) have been corrected by summing up the PUMP4/6-311G($2df$,$2pd$) $O(^1D)-O(^3P)$ energy difference (1.9200 eV) (see text). For a better comparison, the same correction has been performed for experimental data. In parentheses are given, respectively, the adiabatic values of D_e and the added $O(^1D)-O(^3P)$ energy difference for both the experimental and *ab initio* data.

[b]Equilibrium distances for the pseudodiatomic H–(CH_3) and O–(CH_3) molecules correspond to the distances between the atom and the pseudoatom (CH_3) center of mass. See text.

[c]Reference 36 except for the $O(^1D)-O(^3P)$ energy difference (Ref. 47).

[d]From D_0(H–CH_3) of Ref. 48 and taking into account the UMP2/6-311G($2df$,$2pd$) frequencies calculated here for CH_4 and CH_3.

[e]Reference 34.

[f]Estimated from $\Delta H^0_{f,0\,\mathrm{K}}$ of CH_3O used in Ref. 28, and $\Delta H^0_{f,0\,\mathrm{K}}$ of $O(^3P)$ and CH_3 (Ref. 4), assuming D_0 approx. equal to $\Delta H^0_{f,0\,\mathrm{K}}$ and considering the UMP2/6-311G($2df$,$2pd$) frequencies calculated here for CH_3O and CH_3.

[g]R_s, distance between effective nuclear positions derived from isotopic differences in rotational constants (Ref. 37).

(CH_3)OH minimum with the two possible products channels in a H–O–(CH_3) arrangement are shown in Fig. 2.

The root-mean-square deviation (RMSD) for the 126 *ab initio* points fitted is equal to 0.0694 eV (1.60 kcal mol^{-1}). There is also a good agreement between the *ab initio* properties of the stationary points and those resulting from the fitting. The energies (without including ZPE) of the fitted stationary points are, respectively, 0.5 and 0.4 kcal mol^{-1} higher than the *ab initio* values of the saddle point and minimum. These differences are much lower than the global RMSD of the fitting. On the other hand, the largest deviation of the fitted geometries of the stationary points with respect to the *ab initio* ones corresponds to the R_{OH} distance of the saddle point, although it is only equal to 0.07 Å (4.6% of deviation).

Despite of the good agreement that exists between the analytical PES and the *ab initio* calculations, the accord in what respects the energy of the stationary points is not so good when the ZPE is included, as observed in previous triatomic models, see, e.g., Ref. 6. This is due to the fact that the ZPE of CH_4, $O\cdots H\cdots CH_3$ saddle point, CH_3OH minimum, and CH_3 are not properly taken into account in the triatomic model, as the vibrational degrees of freedom of the methyl fragment are neglected. For the analytical PES, the saddle point energy, the minimum depth and the energy of the $OH+CH_3$ and CH_3O+H reaction channels taken from reactants and including ZPE are equal to 2.2, −128.2, −37.7, and −28.9 kcal mol^{-1}, respectively, while in the PUMP4//UMP2 (PUMP4 for the saddle point) *ab initio* calculations these values are obtained: −0.1, −129.2, −42.6, and −28.0 kcal mol^{-1}. The most important effect of the defective description of the energy including ZPE resulting from the model refers to the barrier energy, Thus, while there is no barrier from the *ab initio* data, for the triatomic model a barrier of 2.2 kcal mol^{-1} exists. This should imply the existence of some activation energy for reaction (1), in contrast to what is found in the experiments.[5]

To analyze the influence on the reaction dynamics of the

TABLE VII. Properties of the $O\cdots H\cdots(CH_3)$ saddle point and (CH_3)OH minimum of the analytical triatomic PES.[a]

Stationary point	R_{O-H} /Å	$R_{H-(CH_3)}$ /Å	∠O–H–(CH_3)/ deg	E/kcal mol^{-1}	E + ZPE/kcal mol^{-1}	ν_i /cm^{-1}
Saddle point ($C_{\infty v}$)	1.5832	1.1934	180.0	4.1	2.2	623.7i (Σ^+), 969.4 (Σ^+), 409.2 (Π)
Minimum (C_s)	0.9543	1.9867	46.3	−133.1	−128.2	4014.9 (A'), 1753.4 (A'), 765.2 (A')

[a]Energy referred to reactants.

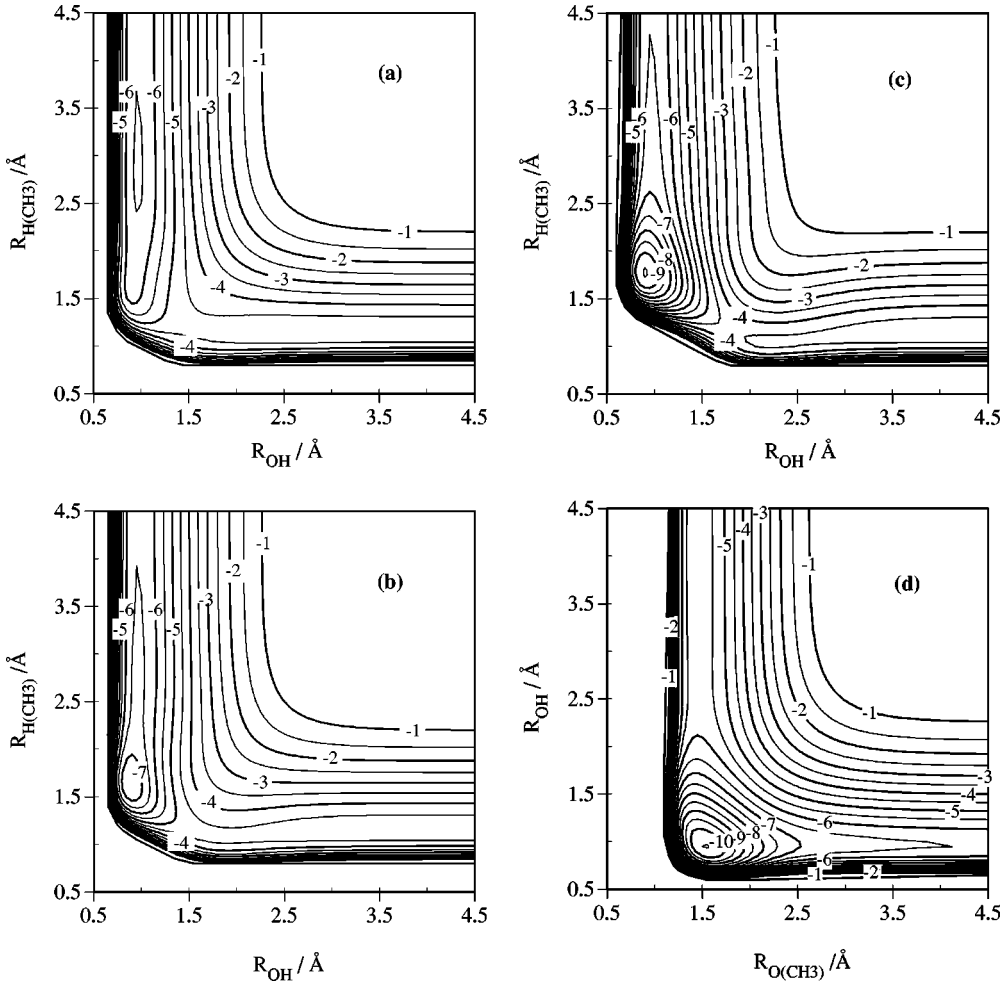

FIG. 2. Equipotential contour diagrams of the analytical triatomic PES; (a) $\angle$O–H–(CH$_3$)=180°; (b) $\angle$O–H–(CH$_3$)=120°; (c) $\angle$O–H–(CH$_3$)=80°; and (d) $\angle$H–O–(CH$_3$)=100°. Energies are given in eV with respect to the dissociated atoms (O(^1D)+H+(CH$_3$)).

existence of a small spurious barrier (when the ZPE is included) in the fully *ab initio* based analytical PES, several analytical PES have been derived by scaling the *ab initio* points around the saddle point region to eliminate the barrier. In this way, it has been shown (see Sec. III) that, disregarding the dependence of the reaction cross section with the collision energy, the dynamical properties considered are not essentially affected by the existence of a small energy barrier. The best of these barrierless analytical PES is available from the authors upon request.

III. QCT DYNAMICS STUDY

The QCT method[49–51] has been applied as implemented in the TRIQCT program[52] considering the analytical triatomic $1\,^1A'$ PES. An integration step of 0.25×10^{-16} s and an initial distance of 10 Å between the O(^1D) atom and the H–(CH$_3$) center of mass have been selected. At this separation the reactants interaction energy can be neglected with respect to the reactants available energy. The rovibrational distribution of the H–(CH$_3$) pseudodiatomic molecule was sampled from a Maxwell–Boltzmann distribution at 298 K.

The QCT dynamics study has been focused on the calculation of the rovibrational distribution of the OH($X\,^2\Pi$) product from reaction (1), because the internal states distribution of this radical is the most widely experimentally characterized dynamics feature of this reaction. Some results on scalar and two-vector properties will also be given. The microscopic reaction mechanism will be analyzed in detail in Sec. III B. To compare QCT rotational populations with the experimental data, as the QCT method does not include neither the orbital ($\Lambda=1$) nor the spin ($S=1/2$) electronic angular momenta of the OH($X\,^2\Pi$) molecule, we have assumed N', the total angular momentum quantum number (excluded the electronic and nuclear spins), to be equal to j', the rotational angular momentum quantum number, plus one.

A. Rovibrational distributions

The measurement of the OH($X\,^2\Pi$) rovibrational distribution arising from reaction (1) has been carried out using several different experimental conditions, concerning mostly the identity of the O(^1D) precursor and wavelength used in its photodissociation (cf. Sec. I). The different conditions yield, in turn, different collision energy distributions for O(^1D)+CH$_4$. In the present QCT calculations we have mainly employed a single relative translational energy (E_T) for the O(^1D)+CH$_4$ system, which corresponds to the average collision energy associated to the O$_3$ photodissociation at 248 nm to yield O(^1D) atoms ($E_T=0.212$ eV using data

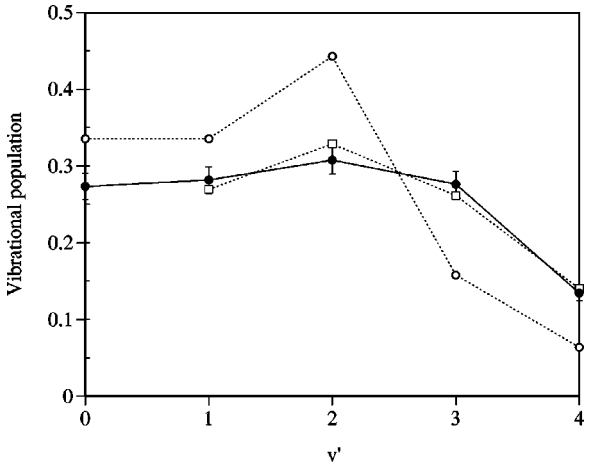

FIG. 3. QCT (●) and experimental (○, Ref. 15 and □, Ref. 13) OH vibrational populations normalized with respect to the sum of the common vibrational levels ($v'=1-4$). The experimental results correspond to the E_T distribution arising from the $O(^1D)$ generated by photodissociation of O_3 at 248 nm. The QCT values result from the corresponding average E_T value (0.212 eV). In all cases the methane molecule was at 298 K.

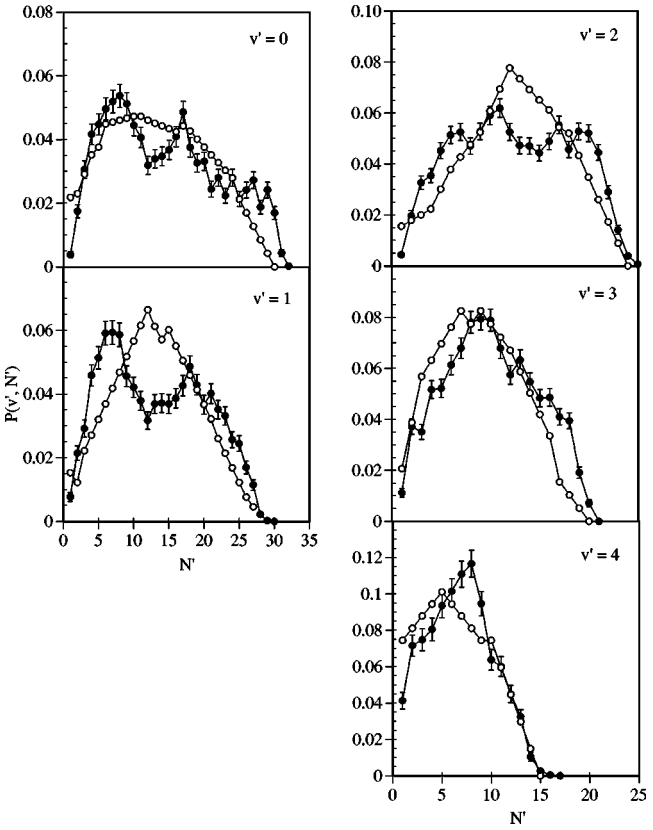

FIG. 4. QCT (●) and experimental (○, Ref. 15) OH rotational distributions. The rotational populations of each vibrational level are normalized to unity. Same comments regarding E_T and the CH_4 molecule as in Fig. 3.

from Ref. 53). The most complete studies about the OH rovibrational distribution have been carried out using O_3 as the $O(^1D)$ precursor. For the photodissociation at 248 nm, two independent experiments[13,15] using different techniques [infrared emission[13] and LIF (Ref. 15)] cover all OH vibrational levels arising from reaction (1).

The QCT OH rovibrational distributions obtained for $E_T=0.212$ eV and H–(CH_3) at 298 K together with the experimental data[13,15] are given in Figs. 3–4 and in Table VIII. From the QCT results it comes out that vibrational levels up to $v'=4$ are populated, being obtained a relatively flat vibrational distribution for $v'=0-3$ that peaks at $v'=2$ (Fig. 3). This is in good agreement with experimental data from Ref. 13. However, QCT data reproduces less accurately the experimental values of Ref. 15, specially in what concerns to $v'=3-4$, because the QCT results, as the experimental ones from Ref. 13, exhibit higher populations for both vibrational levels than in Ref. 15.

There is also a good agreement between the QCT and experimental data[15] when the average OH rotational levels for each vibrational level are compared (Table VIII). The QCT values of the average rotational levels coincide with the experimental data. The agreement is not so good when the QCT and experimental[15] rotational distributions for each vibrational level are compared (Fig. 4), although they still agree quite satisfactorily, particularly for $v'=2-4$. There is a tendency to yield bimodal QCT rotational distributions for $v'=0-2$, which is less evident in the experimental data. The main differences observed between the QCT and experimental[15] rotational distributions appear for the lower vibrational levels ($v'=0$, 1 specially). This could be expected on the basis of the experimental results,[22] which show that the production of OH in the lower vibrational levels is accompanied by internal excitation of the CH_3 radical. The present calculations suggest that the higher excitation of the methyl group should occur when the OH is produced in the lower vibrational levels, as the reactive trajectories are the most complex ones in this case (cf. Sec. III B), so that collision energy could be transferred more efficiently to the CH_3 fragment. Of course, the energy transfer to the CH_3 cannot be accounted for in the framework of a triatomic model where its internal degrees of freedom have been neglected. A comparison between the QCT and experimental[15] rotational distributions by means of the surprisal analysis (see, e.g., Ref. 54) has also been made. From this analysis, it comes out that both the QCT and experimental rotational distributions present a bimodal distribution for $v'=0$, although this behavior is more evident in the former case, as it might be directly concluded from the rotational distributions. No bi-

TABLE VIII. Vibrational populations and average rotational levels of the $OH(X\,^2\Pi)$ molecules arising from the $O(^1D)+CH_4\rightarrow OH+CH_3$ reaction.[a]

	$P(v')/P(v'=1)$ and $\langle N'\rangle_{v'}$				
	$v'=0$	$v'=1$	$v'=2$	$v'=3$	$v'=4$
This work[b]	0.97±0.03	1.00±0.03	1.09±0.03	0.98±0.03	0.48±0.02
	(14.4±1.3)	(13.2±1.1)	(12.5±0.9)	(10.1±0.7)	(6.8±0.6)
Expt.[c]		1.00	1.22	0.97	0.52
Expt.[d]	1.00	1.00	1.32	0.47	0.19
	(13.6)	(12.8)	(12.4)	(8.8)	(6.4)

[a]The first value appearing for each work and vibrational level corresponds to the $P(v')/P(v'=1)$ vibrational population ratio and the one in parentheses gives the average rotational level.
[b]QCT results for $E_T=0.212$ eV and H–(CH_3) at $T=298$ K.
[c]OH rotationally relaxed and Ref. 13.
[d]Reference 15.

modal character appears for the $v'=1$ experimental data, but the $v'=1$ and $v'=2$ QCT rotational distributions are bimodal. For the remaining vibrational levels no bimodal rotational distributions are found neither from QCT nor from experiment. The influence of the microscopic reaction mechanism on the OH energy distribution will be considered in the next section.

The QCT reaction cross section (σ) of $O(^1D)+H-(CH_3)$ (298 K)$\rightarrow OH+(CH_3)$ for $E_T=0.212$ eV is 0.86 Å^2 and increases with E_T. The increase of σ is due to the increase of both the reaction probability (P) and maximum impact parameter (b_{max}). At 0.212 eV $P=5.07\%$ and $b_{max}=2.32$ Å, and the average fraction of energy appearing in products as relative translation ($\langle f'_T\rangle=0.36$), vibration ($\langle f'_V\rangle=0.47$), and rotation ($\langle f'_R\rangle=0.17$) shows a large amount of energy released as OH internal energy, appearing mainly as vibration. A $\mathbf{l}\rightarrow\mathbf{l}'$ angular momentum transformation trend has been observed, with $\mathbf{l}(\mathbf{l}')$ being the reactants (products) orbital angular momentum, according to what can be expected for a reaction with **H–L–H** (heavy–light–heavy) kinematics. Regarding the two-vector properties, the angular distribution (reactive trajectories vs scattering angle) is very broad and has a somewhat larger tendency towards backward scattering (forward/backward (f/b) ratio=0.73), with the initial ($\mathbf{k}$) and final ($\mathbf{k}'$) relative velocity vectors forming an average angle of 95.5°. The OH rotational angular momentum ($\mathbf{j}'$) tends to be perpendicular to both $\mathbf{k}$ and $\mathbf{k}'$, with broad symmetrical distributions around 90°. The $\mathbf{l}'\mathbf{j}'$ distribution is very broad and has a slight tendency to be antiparallel, with an average angle of 104.5°.

Regarding the QCT calculations performed on the PES without any barrier, quite similar results have been found in what concerns the rovibrational distributions of the $OH(X\,^2\Pi)$ molecule: (a) the vibrational distribution for $v'=0-2$ is also relatively flat in this case, although it is not inverted; (b) for $v'=3-4$, the corresponding vibrational populations are lower, even though they still remain between the experimental values of Refs. 13 and 15; (c) the rotational populations derived from the calculations on both types of PES just differ for $v'=0-1$, being obtained a higher rotational excitation when the PES without any barrier are considered (the average rotational levels increase around 20%). Important differences are only observed between the PES with and without barrier when their excitation functions are compared. The QCT reaction cross sections at $E_T=0.212$ eV are at least one order magnitude higher for the barrierless PES and they decrease with E_T.

B. Microscopic reaction mechanism

The analysis of the reactive trajectories (18132) obtained at $E_T=0.212$ eV has allowed us to achieve a deep insight into the microscopic mechanism of reaction (1). The contribution to reaction (1) of the H atom abstraction by the $O(^1D)$ through a direct mechanism, and of the $O(^1D)$ insertion into a C–H bond to yield the CH_3OH intermediate through direct and nondirect mechanisms (see below), have been studied. The lowest energy reached on the ground PES by each reactive trajectory was analyzed [the PES energy of reactants, $OH+(CH_3)$ products and $(CH_3)OH$ minimum are, respectively, −4.79, −6.47, and −10.56 eV]. Only 0.52% of the reactive trajectories evolved from reactants to products with a lowest PES energy higher than −7.0 eV. Regarding the remaining trajectories, the lowest PES energy values reached falls between −7.0 and −9.0 eV (0.55%), between −9.0 and −9.5 eV (5.0%), between −9.5 and −10.0 eV (26.7%) and below −10.0 eV (67.3%). Hence, the $(CH_3)OH$ deep alcohol minimum plays an important role in the dynamics, since nearly all reactive trajectories leading to $OH+(CH_3)$ evolve through geometries close to this minimum. Therefore, reaction (1) takes place near exclusively through the insertion mechanism instead of the abstraction one.

The study of the relationship between the rovibrational distributions and the duration of the collision complex formed through the insertion mechanism is of particular interest. The analysis of the reactive trajectories evolving through insertion, the most relevant ones on the dynamics, evidences the possibility of classifying them in two groups. The first group refers to situations where the lifetime of the $(CH_3)OH$ collision complex can be considered as negligible (direct reaction mechanism (48%)). The second group corresponds to situations where the collision complexes (short lived mainly) exist during several vibrational periods (nondirect reaction mechanism (52%)). The lifetime of the collision complexes ranges from 0.04 to 2.00 ps, the average value is 0.20 ps, and about 80% of nondirect reactive trajectories evolve through $(CH_3)OH$ collision complexes that exist during less than 0.30 ps. Because of the short lifetime values, energy randomization is not allowed. The QCT average lifetime obtained here probably corresponds to a lower limit of the theoretical value which would be obtained if all the degrees of freedom were explicitly accounted for, and can not be compared with the experimental half-collision result of Ref. 26 (3 ps), due to the very different initial conditions considered.

The analysis of the OH rovibrational distribution as a function of the collision complex lifetime does no reveal the existence of important differences. The OH vibrational distribution arising from the direct reaction mode is inverted and has a maximum at $v'=2$. The vibrational populations $P(v'=0):P(v'=1):P(v'=2):P(v'=3):P(v'=4)$ are equal to, respectively, 0.07:0.10:0.13:0.12:0.06. For the nondirect reactive trajectories the distribution is noninverted. $P(v'=0):P(v'=1):P(v'=2):P(v'=3):P(v'=4)$ are equal to, respectively, 0.15:0.12:0.12:0.09:0.05. Regarding the OH rotational distributions, the most relevant results mainly refer to the $v'=0-1$ levels. There is a tendency to give broader rotational distributions peaking at higher N' values in the case of the nondirect trajectories. For $v'=0$ this behavior is responsible for the bimodal rotational distribution obtained in the QCT calculations. For all v' populated, the average rotational level, $\langle N'\rangle$, is in general somewhat larger for nondirect reactive trajectories than for the direct ones. Thus, for the former case and $v'=0-4$ $\langle N'\rangle$ is equal to, respectively, 15.4, 13.9, 12.7, 10.4, 6.9, while for latter one the corresponding values are 11.7, 11.7, 11.9, 9.8, 7.0.

To complete the analysis of the microscopic reaction mechanism of reaction (1), a study of the $OH+CH_3$ branching ratio has been performed. At $E_T=0.212$ eV, 66% of the reactivity is associated with the $OH+CH_3$ products channel. This differs from the 90 $(+10,-20)$% of reactive processes leading to these products measured at room temperature.[7] To understand the origin of this difference, some additional QCT calculations using higher E_T values were carried out, obtaining the following contributions of reaction (1) to the global reactivity; 59%, 53%, and 48% for, respectively, $E_T=0.40$, 0.60, and 0.80 eV. Therefore, there is a clear influence of the collision energy on the products branching ratio, the reaction channel leading to $OH+CH_3$ [reaction (1)] being favored as E_T decreases. This allows to understand the higher $OH+CH_3$ branching ratio experimentally found at room temperature[7] ($\langle E_T\rangle=0.0388$ eV at 300 K) with respect to the QCT calculations at $E_T=0.212$ eV.

A good agreement regarding the reaction microscopic mechanism, the correspondence between rovibrational distribution and microscopic mechanism and the branching ratio is found when the abovementioned results are compared with the ones obtained for the PES without any barrier.

IV. SUMMARY AND CONCLUDING REMARKS

An *ab initio* study of the ground potential energy surface ($1\,^1A'$ PES) of the $O(^1D)+CH_4\rightarrow OH+CH_3$ reaction has been performed using the second and fourth-order Møller–Plesset methods with the 6-311G($2df$,$2pd$) basis set. An $O\cdots H\cdots CH_3$ saddle point and a CH_3OH alcohol minimum have been characterized, and a set of 124 points has been calculated to model the reaction as a triatomic system, with the methyl group treated as an atom of 15.0 amu. The triatomic analytical ground PES based on a many body expansion derived from the *ab initio* points has been employed to study the dynamics of the reaction by means of the QCT method. The QCT dynamics study was focused on the determination of the $OH(X\,^2\Pi,\ v'=0-4,\ N')$ rovibrational distributions found when the 248 nm photodissociation of O_3 is used as $O(^1D)$ precursor. A quite good agreement between the QCT and experimental data has been obtained, both for the relatively flat vibrational distribution, peaked at $v'=2$, and the corresponding rotational distributions. The analysis of the microscopic reaction mechanism shows that the reaction takes place near exclusively through the insertion of the $O(^1D)$ atom into a C–H bond, and the resulting trajectories may be direct or nondirect (mainly through short-lived $(CH_3)OH$ collision complexes) with about the same probability. The OH vibrational distribution arising from the direct mechanism is inverted, while the nondirect mechanism leads to a noninverted distribution. There is some tendency to give broader OH rotational distributions peaking at higher N' values, particularly for the vibrational levels $v'=0-1$, in the case of the nondirect trajectories. At $E_T=0.212$ eV, a reaction branching ratio of 66% is due to the $OH+CH_3$ channel. This value increases as collision energy decreases. The triatomic PES model derived in this work may be used for the study of the dynamics of the title reaction in conditions where the motions of the methyl group are not strongly coupled to the main motions leading to reaction.

As the triatomic model used has a small spurious barrier (including the ZPE) in the analytical PES, additional QCT calculations have been performed on several analytical PES without barrier derived by scaling the *ab initio* points around the saddle point region. Essentially, with the only exception of the excitation function, small differences have been observed with respect to the fully *ab initio* based analytical PES.

ACKNOWLEDGMENTS

This work has been supported by the ''Dirección General de Enseñanza Superior'' of the Spanish Ministry of Education and Culture through the DGES projects PB95-0598-C02-01 and PB95-0598-C02-02. J.H. thanks the CIRIT from the ''Generalitat de Catalunya'' (Autonomous Government), for a predoctoral research grant. The authors are also grateful to the ''Generalitat de Catalunya'' (ref. DGR 1998 SGR 00008) and the University of La Rioja for partial support, and to the ''Center de Supercomputació i Comunicacions de Catalunya (C^4-CESCA)'' for computer time made available.

[1] J. R. Wiesenfeld, Acc. Chem. Res. **15**, 110 (1982).
[2] P. Warneck, *Chemistry of the Natural Atmosphere* (Academic, San Diego, 1988).
[3] E. B. Burnett and C. R. Burnett, J. Atmos. Chem. **21**, 13 (1995).
[4] M. W. Chase, Jr., C. A. Davies, J. R. Downey, Jr., D. J. Frurip, R. A. McDonald, and A. N. Syverud, J. Phys. Chem. Ref. Data **14**, Suppl. 1 (1985).
[5] R. Atkinson, D. L. Baulch, R. A. Cox, R. F. Hampson, Jr., J. A. Kerr, and J. Troe, J. Phys. Chem. Ref. Data **21**, 1215 (1992).
[6] M. González, J. Hernando, J. Millán, and R. Sayós, J. Chem. Phys. **110**, 7326 (1999).
[7] W. Hack and H. Thiesemann, J. Phys. Chem. **99**, 17364 (1995).
[8] S. Satpayal, J. Park, R. Bersohn, and B. Katz, J. Chem. Phys. **91**, 6873 (1989).
[9] Y. Matsumi, K. Tonokura, Y. Inagaki, and M. Kawasaki, J. Phys. Chem. **97**, 6816 (1993).
[10] R. A. Brownsword, M. Hillenkamp, P. Schmiechen, H.-R. Volpp, and H. P. Upadhyaya, J. Phys. Chem. **102**, 4438 (1998).
[11] J. J. Lin, S. Harich, Y. T. Lee, and X. Yang, J. Chem. Phys. **110**, 10821 (1999).
[12] A. C. Luntz, J. Chem. Phys. **73**, 1143 (1980).
[13] P. M. Aker, J. J. A. O'Brien, and J. J. Sloan, J. Chem. Phys. **84**, 745 (1986).
[14] S. G. Cheskis, A. A. Iogansen, P. V. Kulakov, I. Yu. Razuvaev, O. M. Sarkisov, and A. A. Titov, Chem. Phys. Lett. **155**, 37 (1989).
[15] C. R. Park and J. R. Wiesenfeld, J. Chem. Phys. **95**, 8166 (1991).
[16] Y. Rudich, Y. Hurwitz, G. J. Frost, V. Vaida, and R. Naaman, J. Chem. Phys. **99**, 4500 (1993).
[17] M. González, J. Hernando, R. Sayós, M. P. Puyuelo, P. A. Enríquez, J. Guallar, and I. Baños, Faraday Discuss. **108**, 453 (1997).
[18] S. Wada and K. Obi, J. Phys. Chem. **102**, 3481 (1998).
[19] M. Brouard, S. P. Duxon, and J. P. Simons, Isr. J. Chem. **34**, 67 (1994).
[20] M. Brouard and J. P. Simons, The Stereodynamics of Photon Initiated Bimolecular Reactions, in *The Chemical Dynamics and Kinetics of Small Radicals*, edited by K. Liu and A. Wagner (World Scientific, Singapore, 1995), Part II, p. 795.
[21] M. Brouard, H. M. Lambert, J. Short, and J. P. Simons, J. Phys. Chem. **99**, 13571 (1995).
[22] M. Brouard, H. M. Lambert, C. L. Russell, J. Short, and J. P. Simons, Faraday Discuss. **102**, 179 (1995).
[23] J. P. Simons, J. Chem. Soc., Faraday Trans. **93**, 4095 (1997).
[24] T. Suzuki and E. Hirota, J. Chem. Phys. **98**, 2387 (1993).
[25] R. Schott, J. Schlütter, M. Olzmann, and K. Kleinermanns, J. Chem. Phys. **102**, 8371 (1995).
[26] R. D. van Zee and J. C. Stephenson, J. Chem. Phys. **102**, 6946 (1995).
[27] S. P. Walch, J. Chem. Phys. **98**, 3163 (1993).
[28] H. Arai, S. Kato, and S. Koda, J. Phys. Chem. **98**, 12 (1994).

[29] M. J. Frisch, G. W. Trucks, H. B. Schlegel, P. M. W. Gill, B. G. Johnson, M. A. Robb, J. R. Cheeseman, T. Keith, G. A. Petersson, J. A. Montgomery, K. Raghavachari, M. A. Al-Laham, V. G. Zakrzewski, J. V. Ortiz, J. B. Foresman, J. Cioslowski, B. B. Stefanov, A. Nanayakkara, M. Challacombe, C. Y. Peng, P. Y. Ayala, W. Chen, M. W. Wong, J. L. Andres, E. S. Replogle, R. Gomperts, R. L. Martin, D. J. Fox, J. S. Binkley, D. J. Defrees, J. Baker, J. P. Stewart, M. Head-Gordon, C. Gonzalez, and J. A. Pople, GAUSSIAN 94, Revision E.1, Gaussian, Inc., Pittsburgh, Pennsylvania, 1995.
[30] K. A. Peterson and T. H. Dunning, Jr., J. Phys. Chem. A **101**, 6280 (1997).
[31] K. Stark and H. Werner, J. Chem. Phys. **104**, 6515 (1996).
[32] W. Chen and H. B. Schlegel, J. Chem. Phys. **101**, 5957 (1994).
[33] R. Caballol, O. Castell, F. Illas, I. P. R. Moreira, and J. P. Malrieu, J. Phys. Chem. A **101**, 7860 (1997).
[34] Landolt-Börnstein, in *Structure Data of Free Polyatomic Molecules*, edited by K.-H. Hellwege and A. M. Hellwege (Springer-Verlag, Berlin, 1987), Vol. 15 Supplement to Vol. II/7, p. 198.
[35] Experimental frequencies used in Ref. 4 for CH_4 (p. 600) and CH_3 (p. 595) to determine the heat capacity and entropy.
[36] K. P. Huber and G. Herzberg, *Molecular Spectra and Molecular Structure*, Vol. 4, *Constants of Diatomic Molecules* (Van Nostrand Reinhold, New York, 1979).
[37] Landolt-Börnstein, in *Structure Data of Free Polyatomic Molecules*, edited by K. Kuchitsu (Springer-Verlag, Berlin, 1992), Vol. 21 Supplement to Vol. II/7 and II/15, p. 139.
[38] L. A. Curtiss, L. D. Kock, and J. A. Pople, J. Chem. Phys. **95**, 4040 (1991).
[39] T. Shimanouchi, *Tables of Molecular Vibrational Frequencies*, Natl. Stand. Ref. Data Ser. (U.S., Natl. Bur. Stand.) (U.S. GPO, Washington, DC, 1972), Consolidated Vol. I.
[40] J. N. Murrell, S. Carter, S. C. Farantos, P. Huxley, and A. J. C. Varandas, *Molecular Potential Energy Surfaces* (Wiley, New York, 1984).
[41] M. González and R. Sayós, DIATOMFIT (unpublished program).
[42] R. Sayós and M. González, SM3FIT (unpublished program).
[43] M. Gilibert, A. Aguilar, M. González, F. Mota, and R. Sayós, J. Chem. Phys. **97**, 5542 (1992).
[44] M. González, J. Hijazo, J. J. Novoa, and R. Sayós, J. Chem. Phys. **105**, 10999 (1996).
[45] M. González, J. Hijazo, J. J. Novoa, and R. Sayós, J. Chem. Phys. **108**, 3168 (1998).
[46] R. Sayós, J. Hijazo, M. Gilibert, and M. González, Chem. Phys. Lett. **284**, 101 (1998).
[47] S. Bashkin and J. O. Stoner, Jr., *Atomic Energy Levels and Grotrian Diagrams* (North–Holland, Amsterdam, 1975), Vol. 1.
[48] G. Herzberg, *Molecular Spectra and Molecular Structure*, Vol. 3, *Electronic Spectra and Electronic Structure of Polyatomic Molecules* (Van Nostrand Reinhold, New York, 1966).
[49] R. N. Porter and L. M. Raff, in *Dynamics of Molecular Collisions*, edited by W. H. Miller (Plenum, New York, 1976), Part B, p. 1.
[50] D. G. Thuhlar and J. T. Muckerman, in *Atom–Molecule Collision Theory: A Guide for the Experimentalist*, edited by R. B. Bernstein (Plenum, New York, 1979), p. 505.
[51] H. R. Mayne, Int. Rev. Phys. Chem. **10**, 107 (1991).
[52] R. Sayós and M. González, TRIQCT (unpublished program).
[53] M. A. Thelen, T. Gejo, J. A. Harrison, and J. R. Huber, J. Chem. Phys. **103**, 7946 (1995).
[54] D. J. Bogan and D. W. Setser, J. Chem. Phys. **64**, 586 (1976).